Molecular simulation study of the binding mechanism of [α-PTi$_2$W$_{10}$O$_{40}$]$^{7-}$ for its promising broad-spectrum inhibitory activity to FluV-A neuraminidase

WANG JianPing, HU DongHua & SU ZhongMin[*]

Institute of Functional Material Chemistry, Faculty of Chemistry, Northeast Normal University, Changchun 130024, China

Polyoxometalate (POM) has promising antiviral activities. It shows broad-spectrum inhibiting ability, high efficiency, and low toxicity. Experimental assays show that titanium containing polyoxotungstates have anti-influenza-virus activity. In this paper, the binding mechanisms of five isomers of di-Ti-substituted polyoxotungstate, [α-1,2-PTi$_2$W$_{10}$O$_{40}$]$^{7-}$ (α-1,2), [α-1,6-PTi$_2$W$_{10}$O$_{40}$]$^{7-}$ (α-1,6), [α-1,5-PTi$_2$W$_{10}$O$_{40}$]$^{7-}$ (α-1,5), [α-1,4-PTi$_2$W$_{10}$O$_{40}$]$^{7-}$ (α-1,4) and [α-1,11-PTi$_2$W$_{10}$O$_{40}$]$^{7-}$ (α-1,11), to five subtypes of influenza virus A neuraminidase (FluV-A NA) were investigated in the context of aqueous solution by using molecular docking and molecular dynamics studies. The results show that the isomer α-1,2 is superior to other isomers as a potential inhibitor to neuraminidase. The positively charged arginine residues around the active site of NA could be induced by negatively charged POM to adapt themselves and could form salt bridge interactions and hydrogen bond interactions with POM. The binding free energies of POM/NA complexes range from –5.36 to –8.31 kcal mol^{-1}. The electrostatic interactions are found to be the driving force during the binding process of POM to NA. The conformational analysis shows that POM tends to bind primarily with N1 and N8 at the edge of the active pocket, which causes the conformational change of the pincers structure comprising residue 347 and loop 150. Whereas, the active pockets of N2, N9 and N4 are found to be more spacious, which allows POM to enter into the active pockets directly and anchor there firmly. This study shows that negatively charged ligand as POM could induce the reorganization of the active site of NA and highlights POM as a promising inhibitor to NA despite the ever increasing mutants of NA.

influenza virus A, neuraminidase, polyoxometalate, docking, molecular dynamics

Influenza virus can be divided into three genera: A, B and C, based on the antigenic properties of the viral nucleoprotein. Among them, only the influenza virus A (FluV-A) has the ability to cause serious pandemics. It has two surface glycoproteins, hemagglutinin (HA) and neuraminidase (NA), which have been found to have 16 and 9 variants (indicated by H1–H16 and N1–N9), respectively. The three pandemics in history are Spanish pandemic in 1918 caused by FluV subtype H1N1, Asian pandemic in 1957, where HA and NA were replaced by H2 and N2, respectively, and Hong Kong pandemic in 1968, where subtype H3N2 played the main role. In 1997 the new high pathogenic FluV subtype H5N1 appeared in Hong Kong, and later in 2003 it became more fearful [1–7]. It is a top priority to develop new drugs with long-lasting activity, despite the increasing shift and drift of FluV-A. There have been a lot of inhibitors developed to inhibit a broader range of mutants of FluV-A [8,9]. NA inhibitors (NAIs) are considered to be the most valuable and promising in drug market. NA could bind to the sialic acid and cut off the binding interaction of HA and the sialic acid, thus enabling the progeny virions to leave the infected cells and spread to other host cells [3,10]. However, the long-term treatments by the currently available NAI drugs (oseltamivir and zanamivir) triggered out various resistant mu-

*Corresponding author (email: zmsu@nenu.edu.cn)

tants in NA [11–13]. More recently, the drug Peramivir has become attractive for their inhibition to all nine NA subtypes and is at least as active as oseltamivir and zanamivir against H5N1 viruses *in vitro*. However, it has low oral bioavailability in humans. The Phase II study is underway to evaluate single-dose intramuscular peramivir for uncomplicated seasonal influenza [14–16].

There is no appropriate drug with high efficiency and permanent activity in clinical therapy of influenza, especially in combating with the tremendous threat from the forthcoming influenza pandemic. Here we focus on an inorganic-cluster compound, namely polyoxometalate (POM), which is composed of early transition metal cations (usually the d0 species V (V), Nb (V), Ta (V), Mo (VI), and W (VI)) and oxygen anions. It has various interesting properties such as various elemental composition, rich molecular structure, high charge density, controllable redox potential, acidity, and solubility.

For the past three decades, POM has attracted much attention for its antiviral (such as influenza virus, human immunological virus and herpes simplex virus) and anticancer activities [17–23]. It shows potent bioactivity with high efficiency and low toxicity, and is considered to be a broad-spectrum antiviral agent, especially for that containing titanium as a heterometal ion [17,24,25]. In the 1990s, Yamase et al. investigated the antiviral activities of compound $K_7[PTi_2W_{10}O_{40}] \cdot 6H_2O$ (PM-19) and found that PM-19 inhibited HIV replication with more efficiency and lower toxicity than compound $(NH_4)_{17}Na[NaSb_9W_{21}O_{86}] \cdot 14H_2O$ (HPA-23), which was once specified as an anti-HIV drug in France and canceled later for its negatively side effects [26–28]. It was reported that PM-19 potentiated AZT against HIV-1 *in vitro*, but did not potentiate cytotoxicity against MT-4 cells, and its anti-HIV-1 index reached up to 16, the same as that of dextran sulfate [28]. The cytotoxicity of PM-19 to the Vero cells was found to be minimal, with up to 200 μg/mL of PM-19 showing no toxicity. It inhibited several herpes simplex virus (HSV) strains including acyclovir-resistant ones with the value of EC_{50} between 20 and 50 μmol/L [29]. PM-19 was also found to potentiate macrophage activity in both normal and immuno- suppressed mice, and its anti-HSV-2 activity in the latter was even much stronger than that of acyclovir [30]. Another keggin-type titanium containing polyoxotungstate $(PriNH_3)_6$-$H[PTi_2W_{10}O_{38}(O_2)_2] \cdot H_2O$ (PM-523), where Pri is isopropanol, was tested for its therapeutic effectiveness against FluV-A subtype H1N1 infection in tissue culture and in mice with the value of EC_{50} 30 μmol/L, and its combination treatment with ribavirin exhibited synergistic effects but no toxicity [31].

The mechanism of the antiviral activity of POM remains uncertain, although there has been adequate experimental evidence on their *in vitro* bioactivities. The single crystal of POM/protein complex has not been specified in experiments and only some spectral information about the interac-

tions was collected *in vitro* [32–35]. It is necessary to study the binding mechanism of POM at the molecular level to investigate whether there is a strong interaction between POM and the protein, and what the driving force is. The most promising methods to deal with these mechanisms are molecular mechanics (MM) and molecular dynamics (MD) simulations. Sarafianos et al. [36] investigated the mechanism of POM-mediated inactivation of DNA polymerases by docking studies. Hill et al. [37] parameterized Nb-containing POM of the Wells-Dawson class, and docked POM into the HIV-1 protease to discuss their inhibitory mechanism.

In this paper, five isomers of di-Ti-substituted α-keggin polyoxotungstate with Heteroatom Phosphorus ([α-PTi₂W₁₀-$O_{40}]^{7-}$) (Figure 1) were taken as potential inhibitors against five subtypes of NA (N1, N4, N8, N2 and N9). The binding site where POM tended to reside primarily on NA was confirmed *via* molecular docking study. Which isomer of POM had the favorite inhibitory activity was specified according to their binding free energies to NA. The different induced-fit binding processes of POM to the five subtypes of NA were discussed by using flexible docking and MD studies. Then the binding mode and the interaction mechanism were analyzed. In summary, we expect to detect the way in which POM binds to NA, and hope to highlight the broad-spectrum antivirus activity of POM to the various mutants of NA.

1 Computational method

1.1 Calculation strategy

To specify the primary binding site of POM on the surface of NA, software package AutoDock3.0.5 was employed to carry out a rigid docking study. According to the evaluation
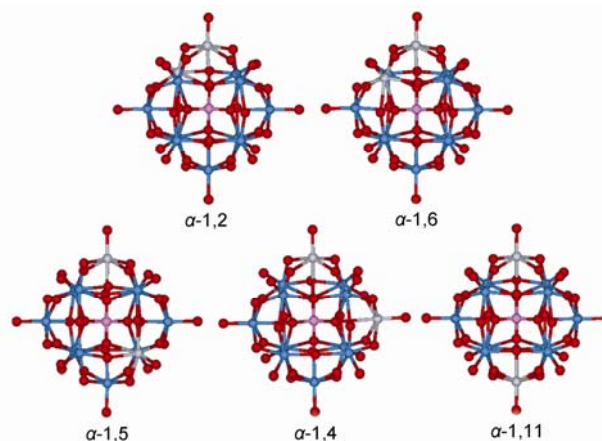
Figure 1 DFT calculated three-dimensional structures of the five isomers of [α-PTi₂W₁₀O₄₀]⁷⁻ are shown in ball-and-stick style. The titanium, tungsten, phosphor, and oxygen elements are indicated by gray, blue, pink, and red balls, respectively. Isomers are defined by the different substituted sites by the two Ti atoms.

by the AutoDock scoring function, the optimal conformation of POM/NA complex was obtained and was subsequently subjected to a flexible docking study to explore the induced-fit binding process of POM into the active pocket of NA. Finally, the stability of POM/NA complex in aqueous solution was explored by using MD simulation study. The flexible docking and MD simulation studies were carried out by using the module Affinity and Discover 3 in Insight II software package (Accelrys Inc., San Diego, CA), respectively.

1.2   Preparation of NA model

Many single crystals of NA have been specified due to the development of the crystallographic study of NA. The veil of the three dimensional structure of NA has been almost disclosed, which bestows us the opportunity to investigate the interactions of NA and their substrates or inhibitors at the molecular level, as well as the precondition of structure-based drug design. NA can be divided into two distinct families, namely group 1 and group 2, in which the former has a 150-cavity adjacent to the active site and undergoes significant rearrangement around loop 150 (composed of residues 147–152) upon binding of substrates and inhibitors [38]. In this study, five subtypes of NA (N1, N2, N4, N8 and N9) belonging to two groups were taken into account, on the one hand to examine the effects resulting from the mutants occurring in the two groups, and on the other hand to investigate the potential broad-spectrum inhibiting activity of POM to NA. The three dimensional structures of the five subtypes of NA were once specified by single-crystal X-ray diffraction method in [38–40] and herein were downloaded from Protein Data Bank (PDB code 2HTY, 2HTV, 2HT5, 2BAT, and 7NN9, for N1, N4, N8, N2, and N9, respectively). NA was added with polar hydrogen and assigned with kollman charges by using the software package AutoDock 3.0 after the crystal water molecules were removed.

1.3   Preparation of POM model

There is no appropriate force field for simulating transition metal elements, and to develop a new force field to depict the dynamics action and molecular mechanics of POM is another giant project [41–45]. Thus, the atomic replacement method developed by Hill et al. seems to be invaluable to investigate the binding mechanism of POM to NA at the molecular level. They intended to develop a protocol for simulating the interaction of POM and the protein [37]. The strategies to realize the rigid docking of POM are stated as follows. First, the rigid structure of POM is faithfully maintained throughout the whole simulation process [46]. Second, MULLIKEN charges (Table S1 on the www.springerlink.com) are assigned to each atom in POM to ensure the better electrostatic interaction [46]. Finally, effective "dummy" atoms are used for

tungsten and titanium. In this investigation, carbon is substituted for tungsten and nitrogen for titanium. The principle of the atomic replacement method is stated in the paper by Hill and co-workers [37].

1.4   Rigid docking study

Rigid molecular docking studies were carried out on the five isomers of ligand POM and the five subtypes of receptor NA. Lamarckian genetic algorithm (LGA) was selected for the ligand conformational search. A 126×126×126 three-dimensional affinity grid centered on the center of the mass of NA with a 0.375 Å grid point spacing was used to calculate the potential maps of the various atom types in POM. The whole NA was enveloped into the grid map to specify the primary binding site where POM inclines to reside on the global surface of NA. There was not any rotatable bond or torsional dihedral angle both in POM and NA. Additional docking parameters were retained as their default values except the parameter *runs value* was changed to 20. As one configuration was solely generated in each run, 20 optimal configurations would be generated at last.

1.5   Flexible affinity of POM/NA complex

It has been demonstrated that incorporating protein structural flexibility is significant for both binding mode predictions and ligand generation [47]. In order to investigate whether the binding process of POM to N1 could be better described by induced-fit theory, we used the module Affinity to implement a flexible docking study on the configuration which had the highest score in the rigid docking. To inspect the induced-fit binding process of POM into the active pocket of NA, the residues in the active pocket and in the vicinity of POM were totally free during the flexible docking simulation as well as in the MD simulation. The flexible region was soaked with two 0.5-nm layers of TIP3P water model to mimic the aqueous solution and the water molecules with a distance of 2.8 Å from POM were removed getting rid of the improper contacts. In order to relax the unrealistic contacts of the inner layer water molecules, we simply minimized the system with all the coordinates of atoms fixed, except for the inner water layer molecules. We consider such a model plausible to simulate the solvent environment in the following two points. First, only the residues in the active pocket of NA were flexible during the simulation. Second, POM had been rigidly docked into the active pocket, with the solvation effect being considered. We just wanted to know the equilibrium conformation of POM in the active pocket in the context of aqueous solution. There are many transition metal atoms in POM, which makes the extensible systematic force field (ESFF) appropriate in modeling such a system. ESFF has the parameters of almost all the elements in the periodic table, and is considered to be able to predict the configuration of organo and

inorganic compounds, though it cannot work out a reasonable energetic evaluation. For the peculiar property of POM in covalent bonding and rigidity, the non-bond cutoff was set to be 20 Å, and POM was tethered with the force constant value 100.0 kcal mol^{-1} Å^2 during the affinity docking process. Energy tolerance was set as 1×10^8 kcal mol^{-1}. The total conformations to generate were set to be 200, and 10 energetically minimal conformations would be ranked with the decent order of the binding free energy in the resultant trajectory. The outer layer water molecules were fixed to ensure that the inner water molecules would not be evaporated out during the flexible docking and MD simulation procedure.

1.6 Molecular dynamics studies of the complexes

The energetically favorable conformation generated from the flexible docking simulation was extracted and subjected to 1 ns MD simulation to specify the equilibrium conformation of the complex in aqueous solution. The solvation effect was modeled as previously mentioned.

2 Results and discussion

2.1 The primary favorable binding site of POM

The binding energies of the five isomers of POM to the five subtypes of NA are listed in Table S2. Isomer α-1,2 shows the strongest affinity to NA (with the binding energy ranging from −0.14 to −3.44 kcal mol^{-1}) for all of the five NA subtypes. Thus isomer α-1,2 could be the most likely NAI. This is consistent with our previous studies. The terminal

oxygens in isomer α-1,2 are most likely to be protonated thereby making isomer α-1,2 more active in the reaction. Isomer α-1,2 manifested the strongest inhibiting activity to the severe acute respiratory syndrome coronavirus 3c like proteinase (SARS-CoV 3CL^{pro}) [46,48]. Zhang et al. claimed that not only does the nominal negative charge of POM appear as a parameter governing the binding process and its consequences, but also the structure, the dimension, molar weight and/or the atomic composition of POM do [32]. According to the cluster analysis there are three possible binding sites for POM on the surface of NA, which are the active pocket, the interface between two NA molecules in a tetramer, and the pore around the four-fold axis of the NA tetramer. The active pocket seems to be the favorite site that POM tends to bind primarily (with the most negative binding energies for almost all of the five NA subtypes). Therefore, the energetically favorable configuration of POM/NA complex in the active-pocket cluster was extracted as the initial conformation of each of the five systems (α-1,2/N1, α-1,2/N2, α-1,2/N4, α-1,2/N8 and α-1,2/N9) in the subsequent studies.

Sequence alignment of the five NA subtypes was realized by software ClustalW 2.0.5 (http://www.ebi.ac.uk/Tools/clustalw2/index.html). The result shows that the five subtypes of NA can be divided into two groups, with N1, N4 and N8 affiliated to group 1, and N2 and N9 to group 2. On the basis of the alignment results, the three dimensional structures of the five subtypes of NA were superimposed (Figure 2). Compared with group 2, NA of group 1 has another pocket adjacent to the active pocket named 150-cavity in the previous study [38]. The 150-cavity is formed by the outward moving of the loop 150.
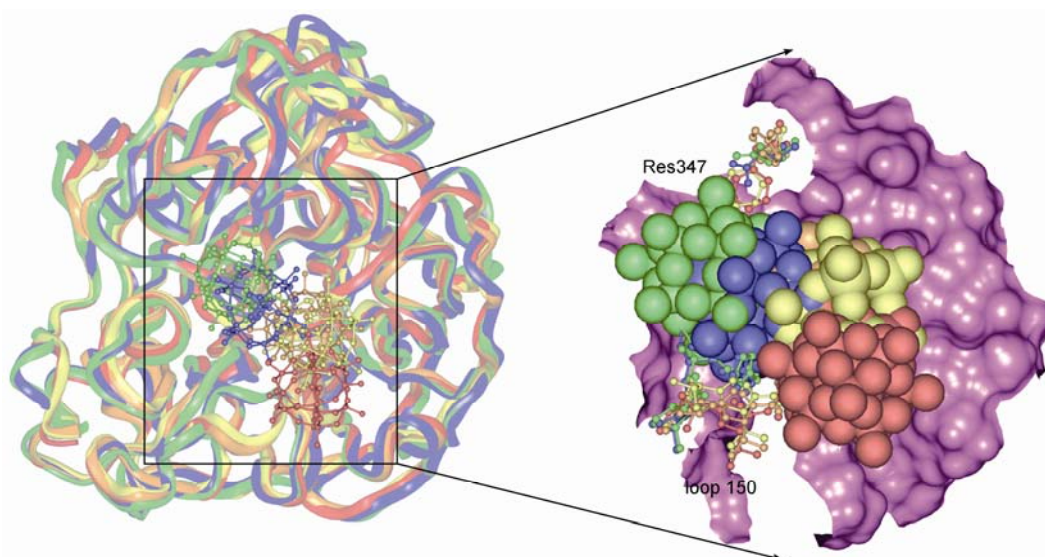
Figure 2   The primary binding modes of the five complexes, α-1,2/N1, α-1,2/N4, α-1,2/N8, α-1,2/N2, and α-1,2/N9, are shown, and NA in each of the five complexes is indicated in yellow, orange, red, green, and blue, respectively, with the corresponding docked POM indicated in the same color. The left panel shows the favorite primary binding sites of the isomer α-1,2 on the surface of NA, with NA rendering ribbon style and POM rendering ball-and-stick style. The right panel indicates the pincers structure, which controls the entry of POM into the active pocket of NA, with the residues comprising the pincers rendering ball-and-stick style and POM rendering CPK style. The Connolly surface of the active pocket of N4 is created to clarify the pincers structure.

The main differences in the binding modes among the five subtypes of NA are attributable to the various conformations and components of residue 347 and loop 150 (Figure 2). Residue 347 and loop 150 act together as pincers to control the entry of POM into the active pocket. A mutant occurred at residue 347 in group 2, with Tyr347Gln and Tyr347Asn in N2 and N9, respectively. In subtypes of group 1 the phenol side chain of Tyr347 is larger than the amide side chain of Gln347 and Asn347 in that of group 2. The difference between subtypes of group 1 and group 2 can also be illustrated as whether there is a 150-cavity [38]. Compared with group 1, there is a mutant Lys150His in the subtype of group 2, and residues 149 and 150 tend to approach to the center of the active pocket, whereas in group 1 they adopt the opposite conformation, which makes the 150-cavity in group 1 (Figure 3). However, the 150-cavity seems to be too large to catch POM tightly, therefore the primary binding mode of POM and NA in group 1 is not stable and may proceed to further dynamic changes. By contrast, POM is able to enter the active pocket of NA in group 2 more deeply and anchor there firmly. The differences of residue 347 in the five subtypes of NA are shown in Figure 4. In group 1, N4 has slightly different features that the phenol side chain rotated out of the pocket almost 120° compared with N1 and N8. Synchronously, the door is opened for POM to enter the active pocket. Thus N4 subtype shows stronger affinity with POM than N1 and N8, and could reach the level of N2 and N9. The phenol side chain of the residue Tyr347 in N1 and N8 tends to protrude into the center of the pocket as a gate refused the entry of POM. In conclusion, POM exhibited different primary binding modes on the surface of the five subtypes of NA, which mainly arose from the mutant of residue 347 and the deviation of the conformation of loop 150 between and within the two groups.
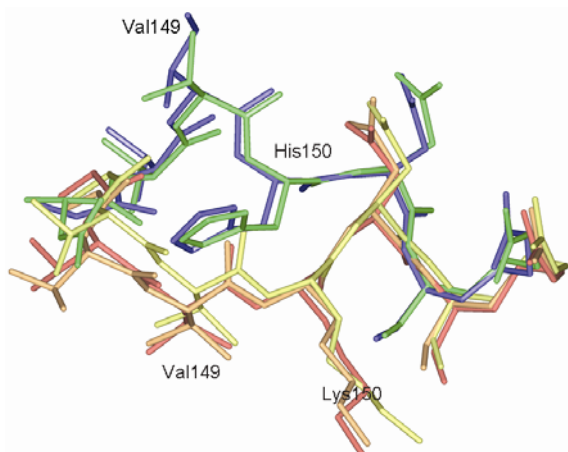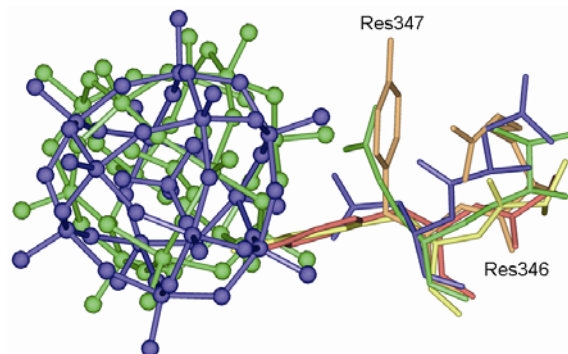
Figure 4 The difference of residue 347, where the mutant happened between group 1 and group 2 and the conformation deviation occurring within group 1, is shown. The isomer α-1,2 docked into N2 and N9 is displayed rendering ball-and-stick style to illustrate the effects of the difference of the conformation of residue 347. Residues 347 and 346 are indicated in sticks. The coloring scheme is the same as in Figure 2.

2.2 The flexible affinity process of POM/NA complex

The ligand may cause conformational changes of a protein as its binding process, especially for highly charged ligand as POM [33,49–52]. The hydrogen bond interactions and key residues in POM/NA complex are shown in Figure 5, and the electrostatic potential maps of NA (N1 and N8) are shown in Figure 6. Figure 5(b) shows that the residue Asp151 is pulled out of the active pocket by forming hydrogen bonds with the near residues such as Gln136 and Gly147. Thus, the door controlled by residue Tyr347 and loop 150 is opened for POM, which then permits POM to enter the active pocket of N1. The positively charged residues, such as Arg430, Arg118, Arg371 and Arg292, approached POM and formed hydrogen bond and salt bridge interactions with negatively charged POM (Figure 5(a)). The electrostatic interactions are shown to be the driving force during the process of the formation of POM/NA complex, which is consistent with the following comparison of the electrostatic potential maps of NA before and after the flexible docking. The pocket of N1 became more spacious and more positively charged after flexible docking (Figure 6). POM was appropriately accommodated in the active pocket of N1 due to steric fitness and electrostatic compatibility.

Compared with N1, subtype N8 has a different conformational change during the flexible docking process. Figure 5(c) shows that the dihedral angle of the two phenyl planes of residue Tyr347 before and after the flexible docking almost reaches 120°. Thus the access of POM into the active pocket is permitted. Simultaneously, the positively charged residues, such as Arg371, Arg118 and Arg152, approached negatively charged POM. The electrostatic potential maps of N8 (Figure 6) show the active pocket becomes more spacious and positively charged compared with the primary active pocket.

For N2, N9 and N4, whose active pockets are found to be more spacious, POM could enter their pocket directly and the residues in the active pocket gradually adopted a more appropriate conformation and orientation to accommodate

Figure 3 The aligned conformations of loop 150 (from residue 147 to 152) in the five subtypes of NA are shown. The residues are shown in stick style and colored by yellow, orange, red, green, and blue for N1, N4, N8, N2, N9, respectively.
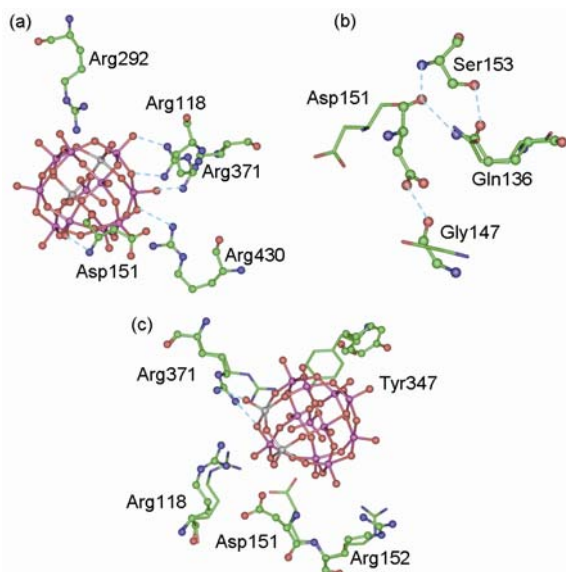
Figure 5 The binding modes of POM/NA complexes before and after flexible docking are shown. (a) and (b) are the hydrogen-bond interactions and the conformational changes of several key residues in α-1,2/N1 complex, respectively. (c) is the hydrogen bond interactions and the conformational changes of several key residues in α-1,2/N8 complex. POM rendered ball-and-stick style. The key residues before and after flexible docking are indicated in stick and ball-and-stick styles, respectively. Hydrogen bonds are indicated by cyan dot lines.
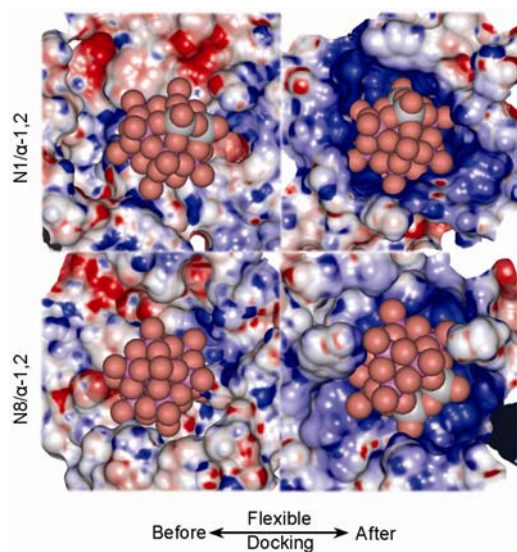
Figure 6 The electrostatic potential maps for the rigid docked NA (N1 and N8) and the flexible docked NA are shown as solid Connolly surface from the top view. The van der Waals surface of POM colored red for oxygen atoms is created to clarify the steric fitness and the electrostatic compatibility between POM and NA in complexes. The surface maps of rigid docked complexes are plotted as in the left half part and that of the flexible docked complex is in the right half part.

POM during the flexible docking simulation. The positively charged residues, Arg371, Arg292 and Arg224 in N2, Arg152 and Arg371 in N9, and Arg152, Arg118 and Arg371 in N4, undertook large movements towards POM,

and formed hydrogen bond and salt bridge interactions with POM.

In summary, POM took an induced-fit process to enter the active pockets of various subtypes of NA in different ways. Electrostatic interactions were found to be the driving force during the binding procedure.

2.3 The equilibrium conformation of POM/NA complex

The highest scored configurations of the five complexes, POM/N1, POM/N2, POM/N4, POM/N8, and POM/N9, were subjected to 1 ns MD simulation. The RMSD values of the configurations of the five NA subtypes are plotted in Figure S1. The snapshots were caught every 500 fs. The RMSD values were all smaller than 1.0, which meant that the conformation of NA had not changed much during the MD simulation. It was shown that all the five complexes were relatively stable in the context of aqueous solution.

Finally, the binding energies of the equilibrium conformations were evaluated in AutoDock3.0.5. The binding energies and the corresponding inhibitory constants are listed in Table 1. The K_i values of the five complexes almost reach the magnitude of μmol/L, which is comparable to the experimental values *in vivo* ($EC_{50} = 30$ μmol L^{-1}) [31]. We did not pay much attention to the fitness of the K_i values between our computational results and that of the experiment，because the metabolism of POM *in vivo* is complex, and the value of EC_{50} could be affected by many factors. The point is that after the induced-fit process POM binds much more strongly (with binding energy ranging from −5.36 to −8.31 kcal mol^{-1}) to NA due to the electrostatic compatibility and geometrical matching.

3 Conclusions

In this paper, we investigated the way in which POM entered the active pocket of NA in the context of aqueous solution by means of molecular mechanics and molecular dynamics simulations. (1) The results of rigid docking of POM to NA subtypes at a global level showed that the isomer α-1,2 had the strongest affinity to NA and the favorable

Table 1 The lowest binding free energies of the five α-1,2/NA complexes and their corresponding inhibitory constants

Complex	E_{low}(kcal mol^{-1})	K_i (μmol L^{-1})
α-1,2/N1	−7.80	1.93
α-1,2/N4	−6.51	16.90
α-1,2/N8	−5.36	119.00
α-1,2/N2	−8.31	0.81
α-1,2/N9	−6.78	10.80

binding site was specified to be the active pocket. It is noteworthy that different binding modes were observed in the five NA subtypes. This could be illustrated by the different configurations or mutants of the residues in the active pocket of the five NA subtypes. The main contributions came from the mutant at 347 and the difference of the conformation of loop 150. (2) It was found that the binding of POM to NA caused the conformational change of the active pocket of NA, thus POM was allowed to enter the active pocket. The highly negatively charged POM induced the near positively charged residues, such as Arg118, Arg292, Arg152 and Arg371, to adapt themselves to a more comfortable position and orientation relative to POM. The electrostatic interactions were the driving force during the binding process of POM into the active pockets of NA. (3) The five POM/NA complexes manifested good stability in aqueous solution, and after the affinity and MD simulation they showed stronger binding energy than the primary binding mode.

It is consistent with the experimental results by Zhang et al. that the binding of POM to proteins may cause the protein molecule to take an unfolding process [49,50]. Highly negatively charged POM could induce the conformational change of NA and form a stronger binding mode. Russell et al. claimed that they had to design new inhibitors for group-1 neuraminidases that are selective for the open loop 150 conformation and would thereby have the potential to bind more strongly than oseltamivir or zanamivir [38]. The selective binding mode of POM onto the loop 150 of NA in group 1 caused the conformational changes of the residues in the active pocket and therefore formed stronger binding affinity. Therefore, we expect POM would become a new generation of anti-influenza virus drug. In summary, in this work we specified a new protocol to theoretically study the induced-fit binding process of POM to proteins at the molecular level. It would be complementary or assistive for experiments in discovering new NAIs.

1   Wingard J R. Facing the next pandemic: Ready or not. Biol Blood Marrow Transplant, 2007, 13: 107–109

2   Trampuz A, Prabhu R M, Smith T F, et al. Avian influenza: A new pandemic threat? Mayo Clin Proc, 2004, 79: 523–530

3   Palese P. Influenza: Old and new threats. Nat Med, 2004, 10: S82–S87

4   Le Q M, Kiso M, Someya K, et al. Avian flu: Isolation of drug-resistant H5N1 virus. Nature, 2005, 437: 1108–1108

5   Ungchusak K, Auewarakul P, Dowell S F, et al. Probable person-to-person transmission of avian influenza A (H5N1). New Engl J Med, 2005, 352: 333–340

6   Guan Y, Poon L L M, Cheung C Y, et al. H5N1 influenza: A protean pandemic threat. Proc Natl Acad Sci USA, 2004, 101: 8156–8161

7   Chen J M, Sun Y X, Liu S, et al. Origin and future distribution of the new A (H1N1) influenza virus emerging in North America in 2009. Chinese Sci Bull, 2009, 54: 2174–2178

8   Smee D F, Huffman J H, Morrison A C, et al. Cyclopentane neuraminidase inhibitors with potent in vitro anti-influenza virus activities. Antimicrob Agents Ch, 2001, 45: 743–748

9   Crusat M, de Jong M D. Neuraminidase inhibitors and their role in avian and pandemic influenza. Antivir Ther, 2007, 12: 593–602

10 De Clereq E, Neyts J. Avian influenza A (H5N1) infection: Targets and strategies for chemotherapeutic intervention. Trends Pharmacol Sci, 2007, 28: 280–285

11 Hurt A C, Ho H T, Barr I. Resistance to anti-influenza drugs: Adamantanes and neuraminidase inhibitors. Expert Rev Anti Infect Ther, 2006, 4: 795–805

12 Kiso M, Mitamura K, Sakai T Y, et al. Resistant influenza A viruses in children treated with oseltamivir: Descriptive study. Lancet, 2004, 364: 759–765

13 Regoes R R, Bonhoeffer S. Emergence of drug-resistant influenza virus: Population dynamic considerations. Science, 2006, 312: 389–391

14 Bantia S, Arnold C S, Parker C D, et al. Anti-influenza virus activity of peramivir in mice with single intramuscular injection. Antivir Res, 2006, 69: 39–45

15 Baum E Z, Wagaman P C, Ly L, et al. A point mutation in influenza B neuraminidase confers resistance to peramivir and loss of slow binding. Antivir Res, 2003, 59: 13–22

16 Yun N E, Linde N S, Zacks M A, et al. Injectable peramivir mitigates disease and promotes survival in ferrets and mice infected with the highly virulent influenza virus, A/Vietnam/1203/04 (H5N1). Virology, 2008, 374: 198–209

17 Barnard D L, Hill C L, Gage T, et al. Potent inhibition of respiratory syncytial virus by polyoxometalates of several structural classes. Antivir Res, 1997, 34: 27–37

18 Shigeta S, Mori S, Watanabe J, et al. Anti-influenzavirus-activities of polyoxometalates. Antivir Res, 1995, 26: A298

19 Rhule J T, Hill C L, Judd D A. Polyoxometalates in medicine. Chem Rev, 1998, 98: 327–357

20 Cindric M, Veksli Z, Kamenar B. Polyoxomolybdates and polyoxomolybdovanadates–from structure to functions: Recent Results. Croat Chem Acta, 2009, 82: 345–362

21 Yamase T. Anti-tumor, -viral, and -bacterial activities of polyoxometalates for realizing an inorganic drug. J Mater Chem, 2005, 15: 4773–4782

22 Hill C L, Weeks M S, Schinazi R F. Anti-HIV-1 activity, toxicity, and stability studies of representative structural families of polyoxometalates. J Med Chem, 1990, 33: 2767–2772

23 Witvrouw M, Weigold H, Pannecouque C, et al. Potent anti-HIV (type 1 and type 2) activity of polyoxometalates: structure-activity relationship and mechanism of action. J Med Chem, 2000, 43: 778–783

24 Liu J, Mei W J, Xu A W, et al. Synthesis, characterization and antiviral activity against influenza virus of a series of novel manganese-substituted rare earth borotungstates heteropolyoxometalates. Antivir Res, 2004, 62: 65–71

25 Shigeta S, Mori S, Yamase T, et al. Anti-RNA virus activity of polyoxometalates. Biomed Pharmacother, 2006, 60: 211–219

26 Rozenbaum W, Dormont D, Spire B, et al. Antimoniotungstate (HPA 23) treatment of three patients with aids and one with prodrome. Lancet, 1985, 325: 450–451

27 Moskovitz B L. Clinical trial of tolerance of HPA-23 in patients with acquired immune deficiency syndrome. Antimicrob Agents Ch, 1988, 32: 1300–1303

28 Take Y, Tokutake Y, Inouye Y, et al. Inhibition of proliferation of human immunodeficiency virus type 1 by novel heteropolyoxotungstates *in vitro*. Antivir Res, 1991, 15: 113–124

29 Fukuma M, Seto Y, Yamase T. *In vitro* antiviral activity of polyoxotungstate (PM-19) and other polyoxometalates against herpes-simplex virus. Antivir Res, 1991, 16: 327–339

30 Ikeda S, Nishiya S, Yamamoto A, et al. Activity of the Keggin polyoxotungstate PM-19 against herpes-simplex virus type-2 infection in

immunosuppressed mice-role of peritoneal macrophage activation. J Med Virol, 1993, 41: 191–195

31 Shigeta S, Mori S, Watanabe J, et al. Synergistic anti-influenza virus A (H1N1) activities of PM-523 (polyoxometalate) and ribavirin in vitro and *in vivo*. Antimicrob Agents Ch, 1997, 41: 1423–1427

32 Zhang G, Keita B, Craescu C T, et al. Molecular interactions between Wells-Dawson type polyoxometalates and human serum albumin. Biomacromolecules, 2008, 9: 812–817

33 Zhang G, Keita B, Craescu C T, et al. Polyoxometalate binding to human serum albumin: A thermodynamic and spectroscopic approach. J Phys Chem B, 2007, 111: 11253–11259

34 Zheng L, Ma Y, Zhang G J, et al. A multitechnique study of europium decatungstate and human serum albumin molecular interaction. Phys Chem Chem Phys, 2010, 12: 1299–1304

35 Zheng L, Ma Y, Zhang G J, et al. Molecular Interaction between a Gadolinium-Polyoxometalate and Human Serum Albumin, Eur J Inorg Chem, 2009, 34: 5189–5193

36 Sarafianos S G, Kortz U, Pope M T, et al. Mechanism of polyoxometalate-mediated inactivation of DNA polymerases: an analysis with HIV-1 reverse transcriptase indicates specificity for the DNA-binding cleft. Biochem J, 1996, 319: 619–626

37 Judd D A, Nettles J H, Nevins N. Polyoxometalate HIV-1 protease inhibitors. A new mode of protease inhibition. J Am Chem Soc, 2001, 123: 886–897

38 Russell R J, Haire L F, Stevens D J. The structure of H5N1 avian influenza neuraminidase suggests new opportunities for drug design. Nature, 2006, 443: 45–49

39 Varghese J N, Epa V C, Colman P M. Three-dimensional structure of the complex of 4-guanidino-Neu5Ac2en and influenza virus neuraminidase. Protein Sci, 1995, 4: 1081–1087

40 Varghese J N, McKimm-Breschkin J L, Caldwell J B, et al. The structure of the complex between influenza virus neuraminidase and sialic acid, the viral receptor. Proteins, 1992, 14: 327–332

41 Comba P. The relation between ligand structures, coordination stereochemistry, and electronic and thermodynamic properties. Coordin Chem Rev, 1993, 123: 1–48

42 Cundari T R, Moody E W, Sommerer S O. Computer-aided design of metallopharmaceuticals: A molecular mechanics force field for gadolinium complexes. Inorg Chem, 1995, 34: 5989–5999

43 Cundari T R, Sisterhen L L, Stylianopoulos C. Molecular modeling of vanadium peroxides. Inorg Chem, 1997, 36: 4029–4034

44 Viloya S A, Christine M K, Clark R L. SHAPES empirical force field: New treatment of angular potentials and its application to square-planar transition-metal complexes. J Am Chem Soc, 1991, 113: 1–12

45 Menke C, Diemann E, Müller A. Polyoxovanadate clusters and cages: Force-field parameterization. J Mol Struct, 1997, 436–437: 35–47

46 Guan W, Yan L K, Su Z M, et al. Electronic properties and stability of dititaniumIV substituted α-Keggin polyoxotungstate with heteroatom phosphorus by DFT. Inorg Chem, 2005, 44: 100–107

47 Alberts I L, Todorov N P, Källbku P, et al. Ligand docking and design in a flexible receptor site. QSAR Combin Sci, 2005, 24: 503–507

48 Hu D H, Shao C, Guan W, et al. Studies on the interactions of Ti-containing polyoxometalates (POMs) with SARS-CoV 3CLpro by molecular modeling. J Inorg Biochem, 2007, 101: 89–94

49 Ajloo D, Behnam H, Saboury A A, et al. Thermodynamic and structural studies on the human serum albumin in the presence of a polyoxometalate. Bull Korean Chem Soc, 2007, 28: 730–736

50 Zhang G, Keita B, Brochon J C. Molecular interaction and energy transfer between human serum albumin and polyoxometalates. J Phys Chem B, 2007, 111: 1809–1814

51 Luong C, Miller A, Barnett J, et al. Flexibility of the NSAID binding site in the structure of human cyclooxygenase-2. Nat Struct Mol Biol, 1996, 3: 927–933

52 Cao Y, Musah R A, Wilcox S K, et al. Protein conformer selection by ligand binding observed with crystallography. Protein Sci, 1998, 7: 72–78

Supporting Information

Table S1   The DFT calculated MULLIKEN charges of the five isomers of $[\alpha\text{-}PTi_2W_{10}O_{40}]^{7-}$.

Table S2   The binding energies of five POMs to five NA subtypes (kcal mol^{-1}).

Figure S1   The RMSD values of the configurations of the five NA subtypes during the 1 ns MD simulation, and the snapshots were caught every 500 fs (for N1 every 1 ps).

The supporting information is available online at csb.scichina.com and www.springerlink.com. The supporting materials are published as submitted, without typesetting or editing. The responsibility for scientific accuracy and content remains entirely with the authors.